

# 1 Evaporation, infiltration and storage of soil water in 2 different vegetation zones in the Qilian Mountains: A 3 stable isotope perspective

4 Guofeng Zhu <sup>a,b\*</sup>, Leilei Yong <sup>a,b</sup>, Zhao Xi <sup>a,b</sup>, Yuwei Liu <sup>a,b</sup>, Zhuanxia Zhang <sup>a,b</sup>, Yuanxiao Xu <sup>a,b</sup>,  
5 Zhigang Sun <sup>a,b</sup>, Liyuan Sang <sup>a,b</sup>, Lei Wang <sup>a,b</sup>

6 <sup>a</sup> *College of Geography and Environment Science, Northwest Normal University, Lanzhou*  
7 *730070, China*

8 <sup>b</sup> *Shiyang River Ecological Environment Observation Station, Northwest Normal University,*  
9 *Lanzhou 730070, Gansu, China*

10 *Correspondence to: Guofeng Zhu (zhugf@nwnu.edu.cn)*

11 **Abstract:** The processes of water storage and runoff generation have not been fully  
12 understood in different vegetation zones in mountainous areas, which is the main  
13 obstacle to further understanding hydrological processes and improving water  
14 resource assessments. To further understand the process of soil water movement and  
15 runoff generation in different vegetation zones (alpine meadow, coniferous forest,  
16 mountain grassland, and deciduous forest) in mountainous areas, this study monitored  
17 the temporal and spatial dynamics of hydrogen and oxygen stable isotopes in the  
18 precipitation and soil water of the Xiyang River Basin. The results show that the  
19 evaporation intensities of the four vegetation zones followed the order of mountain  
20 grassland > deciduous forest > coniferous forest > alpine meadow. The soil water in  
21 the alpine meadows and coniferous forests evaporated from only the topsoil, and the  
22 rainfall input was fully mixed with each layer of soil. The evaporation signals of the  
23 mountain grasslands and deciduous forests could penetrate deep into the middle and  
24 lower layers of the soil as precipitation quickly flowed into the deep soil through the  
25 soil matrix. Each vegetation zone's soil water storage capacity followed the order of  
26 alpine meadow > deciduous forest > coniferous forest > mountain grassland. In  
27 addition, the water storage capacity of shallow soils in different types of vegetation  
28 areas was weaker than that of deep soils. This work will provide a new reference for  
29 understanding soil hydrology in arid headwater areas.

30 **Key words:** Xiying River; Stable isotope; Drought, Soil water storage

## 31 **1. Introduction**

32 In arid inland river basins, changes in climate and vegetation will affect the  
33 hydrological cycle (Tetzlaff et al., 2013; Sharma et al., 2021). As an important  
34 part of the water cycle, soil water in the unsaturated zone can be converted from  
35 precipitation to stream or groundwater recharge. Determining soil water's evaporation,  
36 infiltration, and storage properties is critical for understanding the regional  
37 hydrological cycle and water balance under the background of climate and vegetation  
38 changes (Brooks et al., 2010; Grant and Dietrich, 2017).

39 Isotopes, as "fingerprints" of water, have been used to track ecohydrological  
40 characteristics, such as evaporation (Barnes and Allison, 1988; Zhu et al., 2021b),  
41 groundwater recharge (Koeniger et al., 2016), infiltration paths (Tang and Feng,  
42 2004; Duvert et al., 2016; Zhu et al., 2021a), evapotranspiration distribution  
43 (Xiao et al., 2018; Gibson et al., 2021) and water absorption by plants (Rothfuss  
44 and Javaux, 2017).

45 Water seepage in the unsaturated soil zone and the water evaporation at the air–  
46 soil interface are the main forms of soil water transport. Seasonal variations in  
47 precipitation isotopes are often used to track the process of soil water leakage  
48 (Stumpp et al., 2012). During the piston infiltration process, precipitation with  
49 different  $\delta^2\text{H}$  and  $\delta^{18}\text{O}$  peaks are retained in the soil profile and gradually disappears  
50 as the infiltration depth increases (Sprenger et al., 2016a), while the preferential flow  
51 will keep these peaks until reaching the deep soil layer (Peralta-Tapia et al., 2015).  
52 During a precipitation event, the response of the water isotopes in the surface soil to  
53 precipitation is more obvious, changing to nearly that of the stable isotopes of the  
54 precipitation. With the deepening of the soil layer, the seasonal variation in  
55 precipitation isotope signals rapidly attenuates, and the influence of precipitation on  
56 soil water gradually weakens (Sprenger et al., 2017). Evapotranspiration is the main  
57 form of soil water dissipation. Because the mass of hydrogen and oxygen atoms that  
58 make up water molecules are related to their thermodynamic properties, isotope

59 fractionation of water will occur in the process of the water cycle. The evaporation of  
60 liquid water produces water vapor enriched in  $^1\text{H}$  and  $^{16}\text{O}$ , while the remaining water  
61 is enriched in  $^2\text{H}$  and  $^{18}\text{O}$  (Ferretti et al., 2003). Dansgaard (1964) proposed the  
62 concept of d-excess ( $\text{d-excess}=\delta^2\text{H}-8\delta^{18}\text{O}$ ) to illustrate the intensity of evaporative  
63 fractionation. In the state of isotopic equilibrium, the d-excess is 10. Compared with  
64 d-excess, lc-excess can better explain the evaporative fractionation process. The main  
65 reason is that lc-excess of precipitation and soil water changes smoothly and has  
66 relatively small seasonal changes (Landwehr et al., 2014). The dynamic changes in  
67 isotopes record the signal of soil water evaporation. This enrichment from dynamic  
68 fractionation exists in soil water isotopes in different climatic regions. Compared with  
69 temperate regions, the signals of evaporation in arid and Mediterranean environments  
70 penetrate deeper into the soil (Sprenger et al., 2016b). Some water is stored in the soil  
71 after evaporation and seepage. The water storage capacity of humid areas is higher  
72 than that of arid areas, the water storage capacity of forests is higher than that of  
73 grasslands, and the water storage capacity of the surface soil layer is lower than that  
74 of deeper soil layers with higher clay content (Heinrich et al., 2019; Sprenger et  
75 al., 2019; Kleine et al., 2020; Snelgrove et al., 2021).

76 In alpine mountains, climate warming accelerates the melting of glaciers and  
77 frozen soil, and the dynamic interaction between water bodies stored in different  
78 media becomes the main influence on the water cycle (Penna et al., 2018). Previous  
79 studies on the evaporation, infiltration, and storage of soil water have mostly focused  
80 on different climatic regions or vegetation types in the same climatic region.  
81 Understanding the climatic and hydrological conditions of different vertical  
82 vegetation zones and clarifying the regulating role of vegetation in the water cycle can  
83 help better adapt to climate change's influences on the hydrological cycle in source  
84 areas. This study monitored the stable isotope composition of precipitation and soil  
85 water and the spatiotemporal dynamics of soil water storage in four vegetation zones  
86 (alpine meadow, coniferous forest, mountain grassland, and deciduous forest) with  
87 different hydrothermal conditions in the Xiyang River Basin. To explore the  
88 differences in soil water evaporation, infiltration, and storage processes in these four

89 different climates, vegetation types, and terrain types, the following research  
90 objectives were proposed: (1) to explore the evolution of isotope evaporation signals  
91 and the "memory effects" of precipitation input, mixing and rewetting; and (2) to  
92 understand the soil water storage capacity and influencing factors of four vegetation  
93 areas in mountainous areas.

## 94 **2. Study area**

95 The Xiying River originates from Lenglongling and Kawazhang in the eastern  
96 Qilian Mountains ( $101^{\circ}40'47''\sim 102^{\circ}23'5''E$ ,  $37^{\circ}28'22''\sim 38^{\circ}1'42''N$ ) (Fig. 1). As  
97 the largest tributary of the Shiyang River, it is formed by the Shuiguan River,  
98 Ningchang River, Xiangshui River, and Tatu River converging from southwest to  
99 northeast and ultimately flows into the Xiying Reservoir. The average annual runoff  
100 of the Xiying River is 388 million  $m^3$ , which is mainly replenished by mountain  
101 precipitation and melting water of ice and snow. The runoff is mainly concentrated in  
102 summer. The basin elevation is between 2000 m and 5000 m, corresponding to a  
103 temperate semiarid climate with strong solar radiation, a long sunshine time, and a  
104 large temperature difference between day and night. The average annual temperature  
105 of the basin is  $6^{\circ}C$ , the annual average evaporation is 1133 mm, the annual average  
106 precipitation is 400 mm, and the precipitation from June to September accounts for  
107 69% of the annual precipitation. Precipitation increases with elevation, while  
108 temperature decreases with elevation in this area, (Table 1) (Ma et al., 2018). The  
109 zonal differentiation of vegetation in the basin is dominated by deciduous forest,  
110 mountain grassland, cold temperate coniferous forest, and alpine meadow. The soils  
111 mainly include lime, chestnut, alpine shrub meadow, and desert soil (Fig. 1).

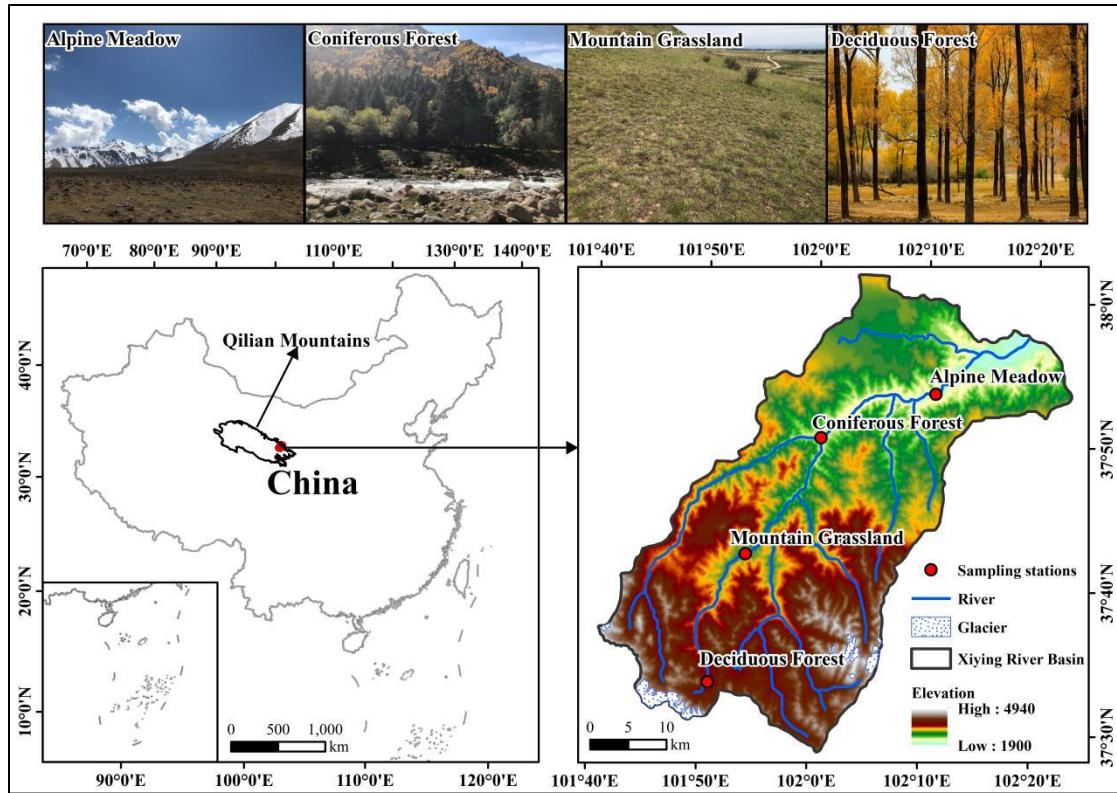


Fig. 1 Study area and location of sampling points

### 3. Data and methods

#### 3.1 Sample collection

In this study, soil water and precipitation samples were collected from four vegetation zones in the Xiyi River Basin from April to October in 2017 (plant growing season). In 2017, the precipitation in the alpine meadows, coniferous forests, mountain grasslands and deciduous forests was 595.1 mm, 431.9 mm, 363.5 mm and 262.5 mm, respectively. The average daily temperatures in the alpine meadows, coniferous forests, mountain grasslands and deciduous forests were  $-0.19^{\circ}\text{C}$ ,  $3.34^{\circ}\text{C}$ ,  $6.6^{\circ}\text{C}$  and  $7.9^{\circ}\text{C}$ , respectively (Table 1).

Collection of soil samples: Soil samples were collected once a month at depths of 0-10, 10-20, 20-30, 30-40, 40-50, 50-60, 60-70, 70-80, 80-90, and 90-100 cm from the soil layers in the four vegetation zones. Three duplicate samples were collected for each soil layer. A collected soil sample was placed into a 50 mL glass bottle, and the bottle mouth was sealed with Parafilm marked with the sampling date; the sample was then frozen for storage until experimental analysis. Each sample was collected separately in an aluminum box.

130 Collection of precipitation samples: The precipitation samples were collected by  
 131 a plastic funnel bottle device. After each precipitation event, the collected  
 132 precipitation samples were immediately transferred to an 80 mL high-density  
 133 polyethylene bottle, and the bottle mouth of the samples was sealed with Parafilm;  
 134 these samples were also frozen and stored until experimental analysis.

135 Meteorological data: During the sampling period, the local meteorological data  
 136 were obtained and recorded by automatic weather stations (Watchdog 2000 series  
 137 weather stations) set up near the sample plot.

138 **Table 1** Basic data of each Vegetation zone from April to October 2017 (*Long*-Longitude,  
 139 *Lat*-Latitude, *Alt*-Altitude, *T*-Air Temperature (daily mean temperature), *P*-Precipitation (total  
 140 precipitation during the observation period), *h*-Relative Humidity (daily mean relative humidity))

Vegetation zone	Geographical parameter			Meteorological parameters			Number of samples	
	<i>Long</i> (°E)	<i>Lat</i> (°N)	<i>Alt</i> (m)	<i>T</i> (°C)	<i>P</i> (mm)	<i>h</i> (%)	Precipitation	Soil
Alpine Meadow	101°51'16"	37°33'28"	3637	-0.19	595.1	69.2	72	47
Coniferous Forest	101°53'23"	37°41'50"	2721	3.34	431.9	66.6	42	41
Mountain Grassland	102°00'25"	37°50'23"	2390	6.6	363.5	60.4	37	54
Deciduous Forest	102°10'56"	37°53'27"	2097	7.9	262.5	59.8	40	53

### 141 3.2 Sample determination

142 The analysis of  $\delta^2\text{H}$  and  $\delta^{18}\text{O}$  values of all the above water samples was  
 143 completed using a liquid water isotope analyzer (DLT-100, Los Gatos Research, USA)  
 144 in the stable isotope laboratory of Northwest Normal University. Before analyzing the  
 145 isotope values of soil water, the soil water was extracted from the collected soil  
 146 samples by a low-temperature vacuum condensation system (LI-2100, LICA United  
 147 Technology Limited, China). Both the water and isotope standard samples were  
 148 injected 6 times during the analysis. To avoid the “memory effect” of isotope analysis,  
 149 we discarded the first two injection values and used the average value of the last four  
 150 injections as the final result (Penna et al., 2012; Qu et al., 2020). The analysis results  
 151 were relative to VSMOW (Vienna Standard Mean Ocean Water):

$$\delta = \left( \frac{R_{\text{sample}}}{R_{\text{standard}}} - 1 \right) \times 1000\text{‰} \quad (1)$$

152 where  $R_{\text{sample}}$  is the ratio of  $^{18}\text{O}/^{16}\text{O}$  or  $^2\text{H}/^1\text{H}$  in the sample and  $R_{\text{standard}}$  is the ratio of  
 153  $^{18}\text{O}/^{16}\text{O}$  or  $^2\text{H}/^1\text{H}$  in the VSMOW. The test error of the  $\delta^2\text{H}$  value does not exceed  
 154  $\pm 0.6\text{‰}$ , and the test error of the  $\delta^{18}\text{O}$  value does not exceed  $\pm 0.2\text{‰}$ .

### 155 3.3 Analysis method

#### 156 3.3.1 Lc-excess

157 The linear relationship between  $\delta^2\text{H}$  and  $\delta^{18}\text{O}$  in precipitation and soil water is  
 158 defined as the LMWL (local meteoric water line) and SWL (soil waterline),  
 159 respectively, are of great significance for studying the evaporative fractionation of  
 160 stable isotopes during the water cycle. We further calculated the line-conditioned  
 161 excess for each soil water and precipitation sample. The lc-excess in different water  
 162 bodies can characterize the evaporation index of different water bodies relative to the  
 163 local precipitation (Landwehr and Coplen, 2006).

$$\text{lc-excess} = \delta^2\text{H} - a \times \delta^{18}\text{O} - b \quad (2)$$

164 where  $a$  and  $b$  are the slope and intercept of the LMWL, respectively, and  $\delta^2\text{H}$  and  
 165  $\delta^{18}\text{O}$  are the isotopic values of hydrogen and oxygen in the sample. The physical  
 166 meaning of lc-excess is expressed as the degree of deviation of the isotope value in  
 167 the sample from the LMWL, indicating the nonequilibrium dynamic fractionation  
 168 process caused by evaporation. Generally, the change in lc-excess in local  
 169 precipitation is mainly affected by different water vapor sources, and the annual  
 170 average is 0. Since the stable isotopes in soil water are enriched by evaporation, the  
 171 average lc-excess is usually negative (Landwehr et al., 2014; Sprenger et al., 2017).

#### 172 3.3.2 Potential evapotranspiration

173 The potential evapotranspiration was calculated based on the Penman-Monteath  
 174 equation (Allen et al., 1998):

$$\text{PET} = \frac{0.408\Delta(R_n - G) + \gamma \frac{900}{T + 273} u^2 (e_s - e_a)}{\Delta + \gamma(1 + 0.34u^2)} \quad (3)$$

175 where PET is the daily potential evapotranspiration ( $\text{mm day}^{-1}$ ),  $R_n$  is the net radiation  
176 ( $\text{MJ m}^2 \text{day}^{-1}$ ),  $G$  is the soil heat flux density ( $\text{MJ m}^2 \text{day}^{-1}$ ),  $\gamma$  is the psychrometric  
177 constant ( $\text{kPa}^\circ\text{C}^{-1}$ ),  $u_2$  is the wind speed at 2 m height ( $\text{m s}^{-1}$ ),  $T$  is the mean daily air  
178 temperature at 2 m height ( $^\circ\text{C}$ ),  $\Delta$  is the slope of the vapor pressure curve ( $\text{kPa}^\circ\text{C}^{-1}$ ),  $e_a$   
179 is the actual vapor pressure (kPa) and  $e_s$  is the saturated vapor pressure (kPa). These  
180 data come from nearby weather stations.

### 181 3.3.3 Soil water storage

182 Soil water storage is the thickness of the water layer formed by all the water in a  
183 certain soil layer (Milly, 1994) and is expressed by the following formula:

$$S = R \times W \times H \times 10 \quad (4)$$

184 where  $S$  is the soil water storage in a certain thickness layer (mm),  $R$  is the soil bulk  
185 density ( $\text{g cm}^{-3}$ ), and  $H$  is the soil thickness (cm).  $W$  is the gravimetric water content,  
186 which is expressed by the following formula:

$$W = \frac{M_1 - M_2}{M_2} \times 100\% \quad (5)$$

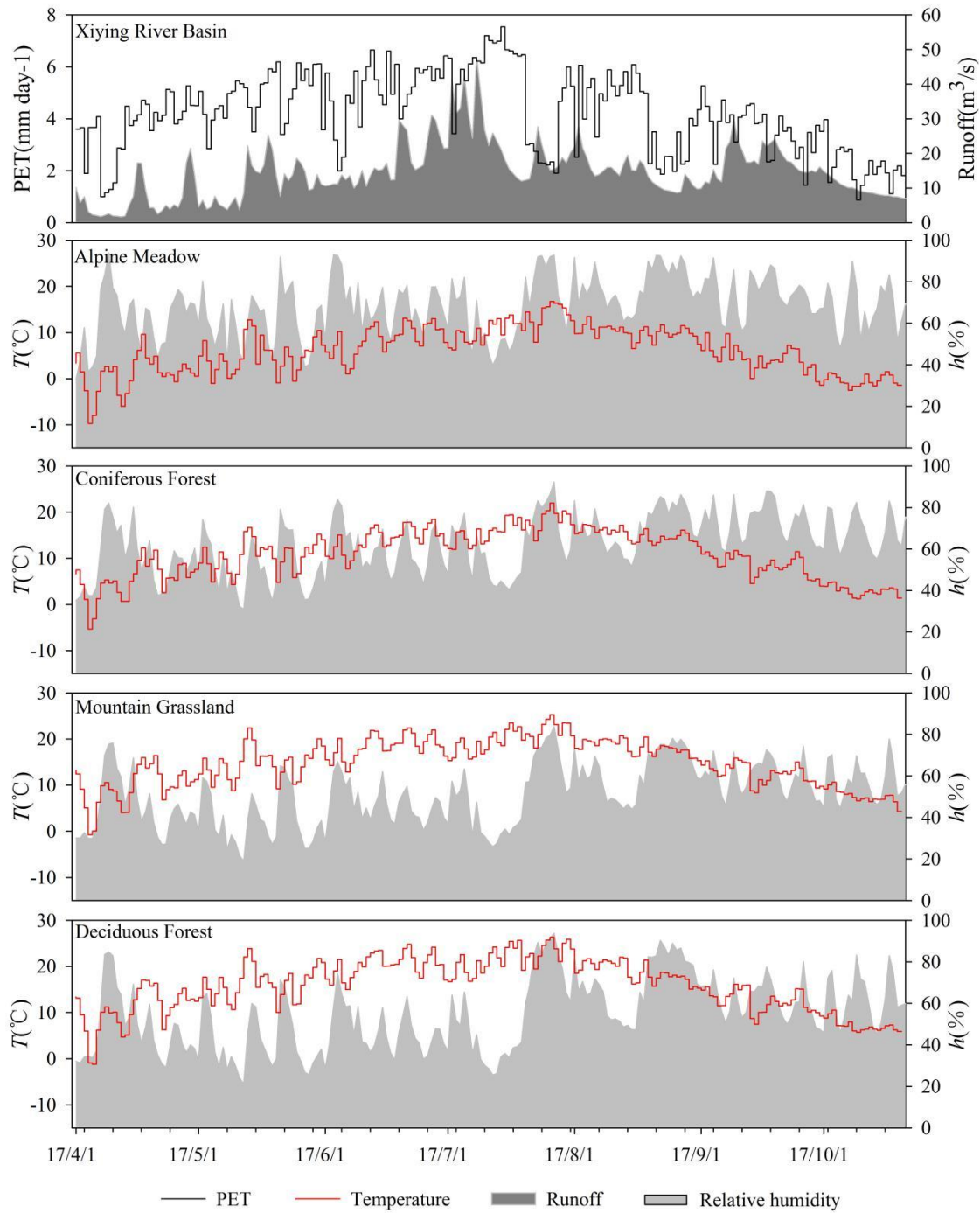
187 in the formula,  $M_1$  is the gravimetric value of wet soil (g), and  $M_2$  is the gravimetric  
188 value of dry soil (g).

## 189 4. Results and analysis

### 190 4.1 Hydrological climate

191 PET and runoff are important indicators that reflect the dry-wet conditions of  
192 river basins. During the study period (April-October 2017), in the Xiying River Basin,  
193 the potential evapotranspiration was 872.8 mm, the daily evapotranspiration ranged  
194 from 7.5 mm (July 14) to 0.9 mm (October 9), showing a fluctuating trend around  
195 July, and the PET value in April-July was higher than that in August-October. The  
196 input of summer precipitation and ice/snow meltwater increased runoff, resulting in a  
197 trend similar to PET. During the observation period, the total runoff was  $3.1 \times 10^9$  m,  
198 accounting for 89% of the annual runoff. The variation range of the daily runoff was  
199  $286848 \text{ m}^3$  (April 17) to  $6125760 \text{ m}^3$  (July 13). The basin before July was drier than  
200 that after July (Fig. 2).





201

202 **Fig. 2** Climatic and hydrological conditions of Xiying River basin and its vegetation  
 203 zones

204 To explore the differences in the natural environment in different vegetation  
 205 zones, air temperature, atmospheric humidity, and precipitation were used to indicate  
 206 each research site's temperature and moisture conditions. The hilltop is a typical  
 207 alpine meadow zone, with a daily average temperature of 6.1°C, ranging from -9.7°C

208 (April 5) to 16.8°C (July 27). The daily average humidity was 68.2%, with little  
209 difference in different periods. During the observation period, there were 72  
210 precipitation events in the alpine meadow zone, and the total precipitation was 534.3  
211 mm, which was relatively evenly distributed each month. In the coniferous forest zone,  
212 the daily average temperature during the study period was 10.9°C, ranging from  
213 -5.4°C (April 5) to 22.0°C (July 27). The daily average humidity was 62.5%, and the  
214 precipitation was 400.6 mm, mainly concentrated from early August to late September.  
215 Close to the foothills is the mountain grassland zone, with a daily average temperature  
216 of 14.9°C, ranging from -0.7°C (April 5) to 25.3°C (July 27). The average daily  
217 humidity was 51.1%, and the precipitation of the vegetation zone during the  
218 observation period was 327.2 mm, mainly from late July to mid-August. During the  
219 observation period, the daily average temperature in the deciduous forest zone was  
220 15.8°C, ranging from -1.2°C (April 6) to 26.3°C (July 27). The daily average  
221 humidity was 54.7%, and the total precipitation was 250.6 mm, which was  
222 concentrated in the month from late July to late August. The temperatures of the  
223 studied regions were ordered as follows: AM (alpine meadow) < CF (coniferous  
224 forest) < MG (mountain grassland) < DF (deciduous forest). The humidities of the  
225 studied regions were ordered as follows: AM > CF > MG > DF (Fig. 2).

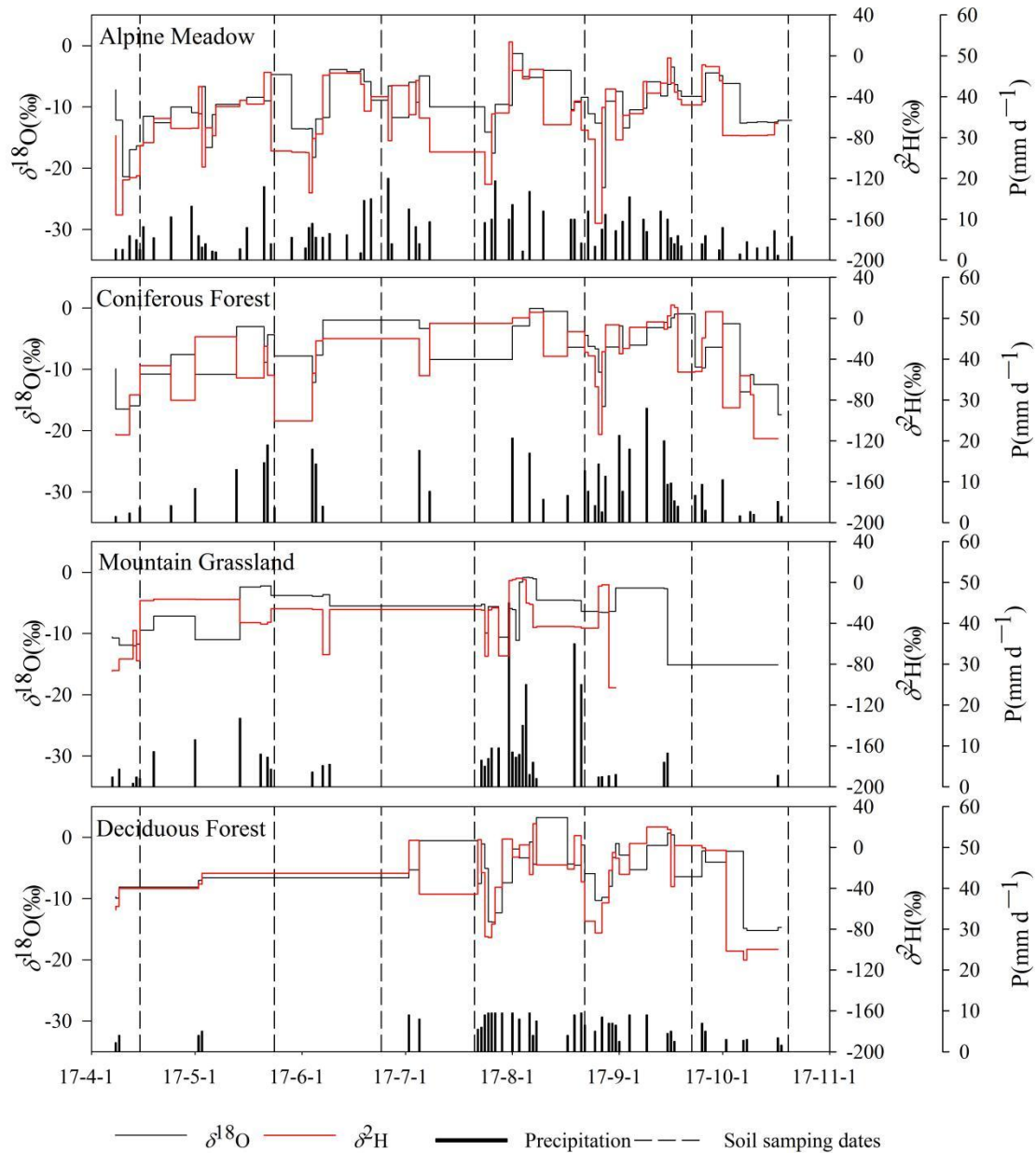
#### 226 **4.2 Temporal variation in water stable isotopes in different vegetation zones**

227 Influenced by different water sources and complex weather conditions in the  
228 precipitation process, the isotopic compositions of precipitation in the four vegetation  
229 zones were different during the study period. The mean values of  $\delta^2\text{H}$  and  $\delta^{18}\text{O}$  in the  
230 alpine meadow zone (number of samples: 72) were  $-73.1\text{‰}\pm 36.3\text{‰}$  (-163.9~13.7‰)  
231 and  $-10.0\text{‰}\pm 4.3\text{‰}$  (-23.1~-1.3‰), respectively. The average  $\delta^2\text{H}$  and  $\delta^{18}\text{O}$  values of  
232 the coniferous forest zone (number of samples: 42) were  $-42.0\text{‰}\pm 37.2\text{‰}$   
233 (-117.8~13.0‰) and  $-7.1\text{‰}\pm 4.7\text{‰}$  (-17.4~-0.1‰), respectively. The average  $\delta^2\text{H}$  and  
234  $\delta^{18}\text{O}$  values of the mountain grassland zone (number of samples: 37) were  
235  $-37.4\text{‰}\pm 30.5\text{‰}$  (-103.1~4.2‰) and  $-5.9\text{‰}\pm 3.9\text{‰}$  (-15.1~-0.9‰), respectively. The  
236 average  $\delta^2\text{H}$  and  $\delta^{18}\text{O}$  values of the deciduous forest zone (number of samples: 40)  
237 were  $-31.8\text{‰}\pm 42.8\text{‰}$  (-110.2~23.2‰) and  $-5.8\text{‰}\pm 5.5\text{‰}$  (-15.2~3.2‰), respectively

238 (Table 2). The maximum isotopic values of the four vegetation zones appeared on  
 239 August 4 (AM: 13.7‰,  $\delta^2\text{H}$ ; -1.3‰,  $\delta^{18}\text{O}$ ), August 10 (CF: 13.0‰,  $\delta^2\text{H}$ ; -0.1‰,  
 240  $\delta^{18}\text{O}$ ), August 7 (MG: 4.2‰,  $\delta^2\text{H}$ ; -0.9‰,  $\delta^{18}\text{O}$ ) and August 13 (DF: 23.2‰,  $\delta^2\text{H}$ ;  
 241 3.2‰,  $\delta^{18}\text{O}$ ). The highest temperature in each vegetation zone appeared on July 27.  
 242 The high temperature caused the precipitation to undergo strong below-cloud  
 243 evaporation during the fall, leading to the enrichment of isotopes. In addition, the  
 244 atmospheric precipitation isotopes of the four vegetation zones had similar temporal  
 245 variations: from April to August, the fluctuations in  $\delta^2\text{H}$  and  $\delta^{18}\text{O}$  increased, reached  
 246 the maximum in mid-August, and then gradually decreased (Fig. 3).

247 **Table 2** General characteristics of precipitation  $\delta^2\text{H}$  and  $\delta^{18}\text{O}$  in different vegetation areas  
 248 from April to October 2017

Vegetation zone	$\delta^2\text{H}/\text{‰}$				$\delta^{18}\text{O}/\text{‰}$			
	Max	Min	mean	SD	Max	Min	mean	SD
AM	13.7	-163.9	-73.1	36.3	-1.3	-23.1	-10.0	4.3
CF	13.0	-117.8	-42.0	37.2	-0.1	-17.4	-7.1	4.7
MG	4.2	-103.1	-37.4	30.5	-0.9	-15.1	-5.9	3.9
DF	23.2	-110.2	-31.8	42.8	3.2	-15.2	-5.8	5.5



249

250 **Fig. 3** Time series of rainfall and isotope characteristics in different vegetation  
 251 zones in Xiying River Basin, with dotted lines indicating the date of soil water  
 252 sampling

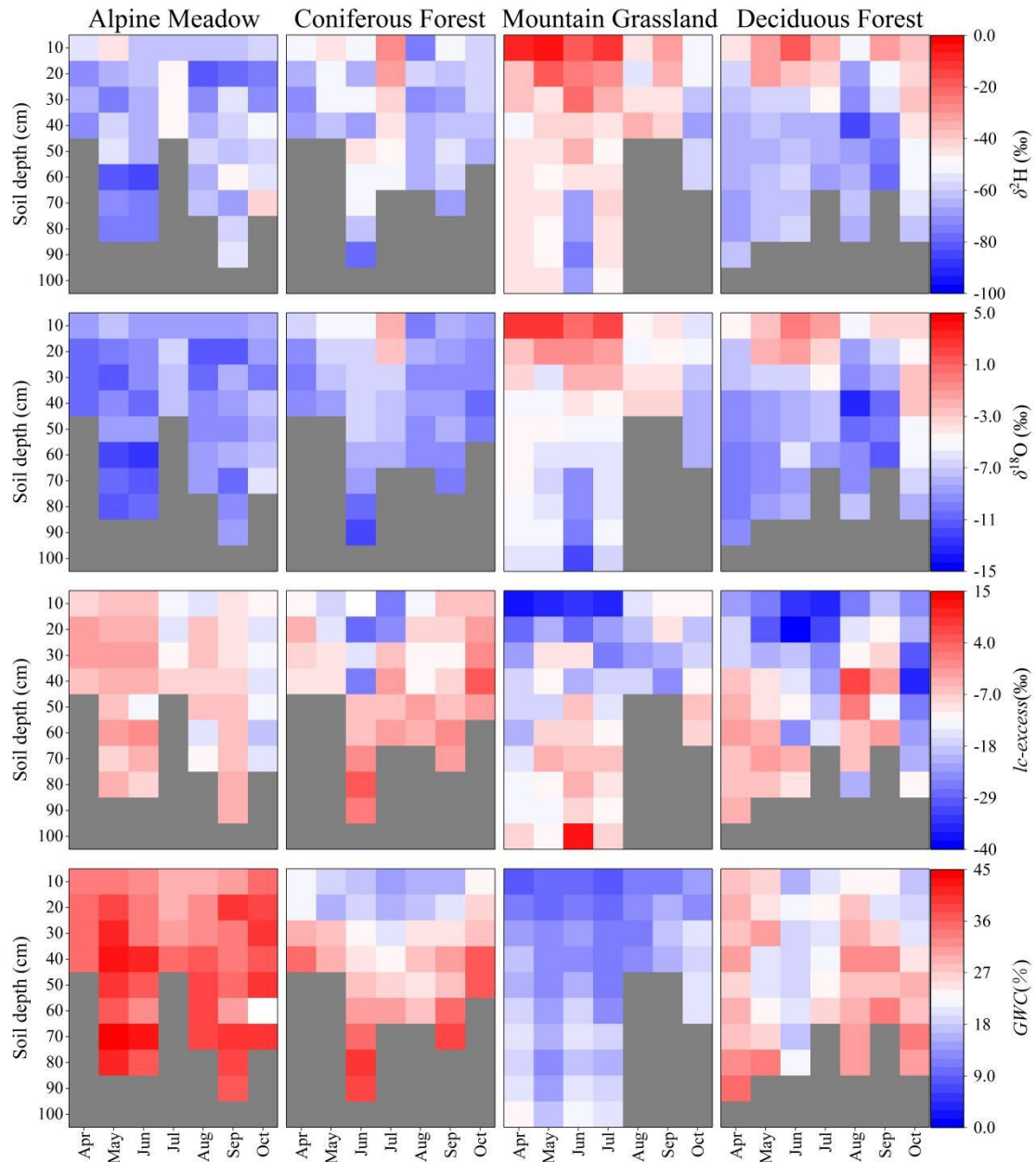
253 The monthly variation in soil water isotopes records the signal of precipitation  
 254 input and evaporation. The low-temperature environment and abundant precipitation  
 255 events in the alpine meadows make the monthly average  $\delta^2\text{H}$  and  $\delta^{18}\text{O}$  of soil water  
 256 more depleted than other vegetation zones ( $-69.4\sim-51.6\text{‰}$ ,  $\delta^2\text{H}$ ;  $-7.5\sim-10.3\text{‰}$ ,  $\delta^{18}\text{O}$ ).  
 257 Despite this, the SWlc-excess of most samples at this station was still negative, and  
 258 there were different degrees of evaporation in the process of precipitation penetrating

259 the soil and mixing with original pore water, among which evaporation fractionation  
260 was stronger in July (-11.9‰ lc-excess) and October (-14.5‰ lc-excess). The soil  
261 water isotopes of the coniferous forests gradually changed seasonally. From April to  
262 July, precipitation was scarce, the temperature rose, and the isotopes of soil water  
263 were gradually enriched on the surface (-52.7~-29.5‰,  $\delta^2\text{H}$ ; -7.0~-2.1‰,  $\delta^2\text{H}$ ),  
264 reaching the peak value of the observation period in July (-29.5‰,  $\delta^2\text{H}$ ; -2.1‰,  $\delta^{18}\text{O}$ ),  
265 and continuous rainfall input from late July to mid-August resulted in soil water  
266 isotope depletion (-57.0‰,  $\delta^2\text{H}$ ; -8.1‰,  $\delta^{18}\text{O}$ ). SWlc-excess was an obvious  
267 fractionation signal opposite to the trend of isotope change, reaching the lowest value  
268 (-26.3‰) in the sampling period in July, and the change in air temperature and  
269 precipitation controlled the evaporation intensity. From April to July, the isotopic  
270 value of surface soil water in the mountain grasslands was higher ( $\delta^{18}\text{O}$  was greater  
271 than zero), and SWlc-excess was lower than -30‰. During this period, the  
272 evaporation and fractionation of shallow soil water were intense. Similar to in the  
273 coniferous forests, in the mountain grasslands, the input of heavy precipitation from  
274 late July to mid-August led to the depletion of soil water isotopes. There was only  
275 sporadic rainfall in the deciduous forests from April to July, and the soil water  
276 isotopes were gradually enriched on the surface (-46.1~-18.2‰,  $\delta^2\text{H}$ ; -4.7~0.2‰,  
277  $\delta^2\text{H}$ ), reached a peak in June when there was no rainfall event (-18.2‰,  $\delta^2\text{H}$ ; 0.2‰,  
278  $\delta^{18}\text{O}$ ), and then became depleted (-53.2‰,  $\delta^2\text{H}$ ; -5.2‰,  $\delta^{18}\text{O}$ ). In addition, due to the  
279 influence of the Xiyang Reservoir and vegetation coverage, the isotopic enrichment  
280 degree of soil water in this vegetation zone was lower than that in the mountain  
281 grasslands. As the most intuitive form of water change, the gravimetric water content  
282 was always at a low value in July (AM: 21.0; CF: 14.8; MG: 11.9; DF: 14.9), when  
283 the evaporation was the strongest, and it was most obvious in shallow soil (Table 3)  
284 (Fig. 4).

285  
286  
287

vegetation areas from April to October 2017

Month	Vegetation zone	$\delta^2\text{H}/\text{‰}$			$\delta^{18}\text{O}/\text{‰}$			lc-excess/ $\text{‰}$			GWC/ $\text{‰}$		
		Max	Min	Mean	Max	Min	Mean	Max	Min	Mean	Max	Min	Mean
4	AM	-55.2	-70.7	-65.6	-8.5	-10.8	-10.1	-2.7	-7.1	-4.7	25.9	23.0.0.	24.7
	CF	-52.7	-72.2	-63.9	-7.0	-9.9	-8.9	-4.0	-12.0	-8.4	27.6	14.9	20.0
	MG	-7.32	-50.6	-41.0	2.8	-5.8	-3.9	-8.8	-36.8	-19.4	21.7	6.5	14.7
	DF	-46.1	-69.4	-62.1	-4.7	-9.9	-8.5	-2.5	-23.2	-9.7	27.7	19.4	21.8
5	AM	-46.1	-76.5	-66.4	-7.4	-12.2	-10.1	-2.6	-7.7	-4.9	32.6	23.2	28.9
	CF	-45.8	-61.9	-53.5	-5.3	-8.4	-7.0	-9.3	-17.7	-13.0	22.6	9.0	16.1
	MG	-6.7	-47.3	-39.2	2.9	-6.5	-4.3	-4.5	-36.2	-14.4	15.7	7.6	11.2
	DF	-30.8	-63.5	-53.8	-1.9	-9.4	-6.9	-3.2	-30.1	-13.6	26.0	11.7	17.7
6	AM	-62.5	-83.9	-69.4	-8.9	-12.6	-10.3	-1.5	-8.4	-5.8	33.3	21.9	26.0
	CF	-45.8	-78.4	-58.7	-5.1	-12.0	-7.8	5.5	-26.6	-8.5	32.1	10.0	21.3
	MG	-19.7	-74.9	-46.9	0.8	-11.8	-5.8	13.0	-33.7	-11.0	19.3	7.5	14.2
	DF	-18.2	-64.9	-51.7	0.2	-9.0	-5.9	-4.6	-38.2	-19.4	13.5	8.4	11.1
7	AM	-47.3	-60.1	-51.6	-6.9	-8.4	-7.5	-8.8	-14.8	-11.9	25.4	19.0	21.0
	CF	-29.5	-51.4	-41.6	-2.1	-7.9	-5.6	-2.6	-26.3	-11.2	24.3	7.2	14.8
	MG	-10.6	-48.4	-39.2	2.3	-6.4	-4.1	-5.8	-35.8	-16.1	18.7	6.3	11.9
	DF	-35.1	-69.0	-54.1	-1.7	-8.7	-5.5	-14.8	-35.3	-24.5	18.2	11.8	14.4
8	AM	-58.5	-80.3	-66.6	-8.4	-11.6	-9.6	-6.1	-15.4	-9.7	28.1	19.5	25.1
	CF	-57.0	-75.5	-66.4	-8.1	-9.8	-9.2	-2.5	-13.1	-8.3	21.4	8.7	16.3
	MG	-34.2	-53.8	-44.0	-3.2	-5.5	-4.4	-14.7	-22.6	-18.7	11.3	9.5	10.4
	DF	-53.2	-84.3	-67.6	-5.2	-13.5	-9.2	6.8	-26.1	-9.6	23.6	14.7	20.6
9	AM	-48.0	-79.2	-61.0	-7.8	-11.1	-9.2	-4.3	-10.4	-7.2	29.9	20.3	25.3
	CF	-52.5	-67.7	-60.7	-7.8	-10.1	-8.8	-0.1	-11.3	-6.0	31.3	9.3	20.5
	MG	-32.3	-45.3	-38.8	-3.5	-4.4	-4.0	-9.1	-23.8	-16.5	15.3	9.1	13.0
	DF	-30.5	-77.0	-59.8	-3.1	-11.4	-8.2	-1.8	-19.3	-9.3	25.8	14.7	19.1
10	AM	-42.4	-73.5	-58.9	-6.1	-9.8	-7.9	-12.2	-18.2	-14.5	36.2	25.4	29.5
	CF	-59.1	-66.3	-61.7	-8.8	-10.5	-9.5	5.1	-5.3	-1.5	30.0	16.8	23.1
	MG	-50.3	-66.7	-58.3	-5.6	-8.3	-7.1	-5.5	-18.4	-11.9	18.3	11.4	15.8
	DF	-38.0	-61.8	-48.3	-2.7	-8.2	-4.9	-11.9	-34.8	-23.9	25.5	8.9	17.2



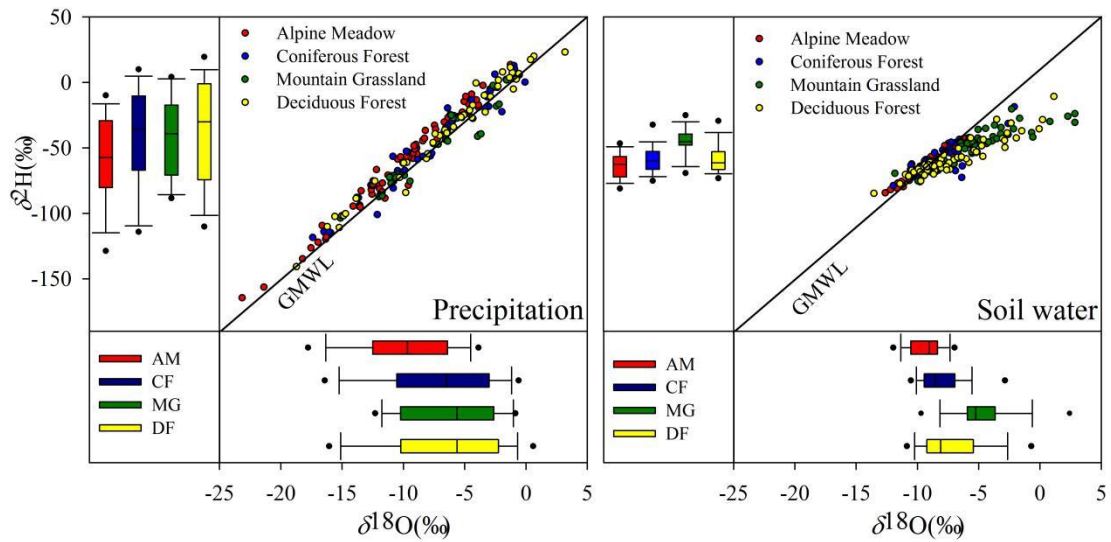
290

291 **Fig. 4** Heat map of the soil depth profile of  $\delta^2\text{H}$ ,  $\delta^{18}\text{O}$ , lc-excess and GWC in  
 292 different vegetation zones, and the layer lacking measurement is indicated by grey  
 293 color

294 **4.3 Spatial variation in water stable isotopes in different vegetation zones**

295 Isotope data of precipitation and soil water obtained from different vegetation  
 296 zones are shown in dual-isotope space in Fig. 5. At the alpine meadow observation  
 297 station, the slope (8.4) and intercept (23) of the LMWL were higher than those of the  
 298 GMWL. The slope of the LMWL in the other three vegetation zones was lower than  
 299 that of the GMWL and gradually decreased with decreasing altitude. With the

300 decrease in altitude, the slope of the SWL in all vegetation zones except for the  
 301 deciduous forest SWL decreased (AM: 6.4; CF: 4.7; MG: 3.4; DF: 4.1), indicating  
 302 that the evaporation of soil moisture increased. On the one hand, the vegetation  
 303 coverage of the deciduous forest site was higher. On the other hand, the Xiying  
 304 Reservoir enhanced the regional air humidity and decreased the local water vapor  
 305 circulation driving force.



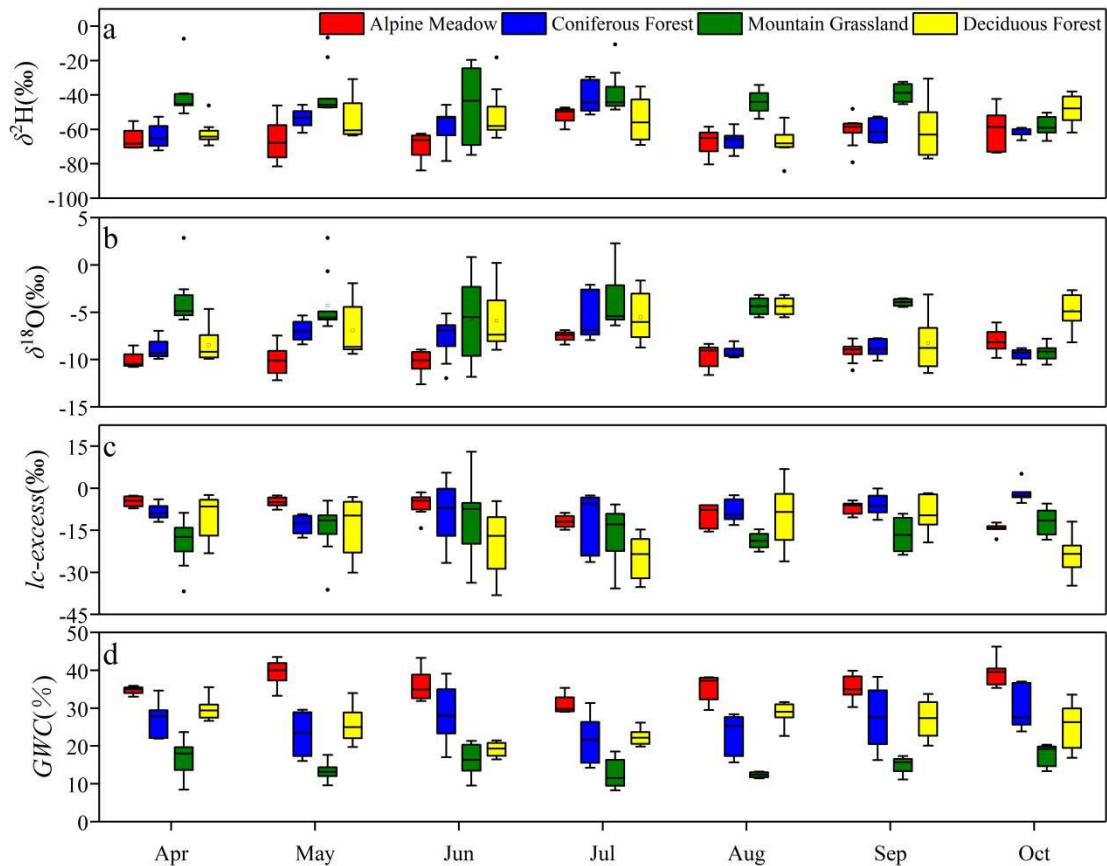
306

307 **Fig. 5** Dual-isotope space of precipitation (left) and soil water (right) isotope data of  
 308 four vegetation zones. In the box plots, the box represents 25%-75% percentile, the  
 309 line in the box represents median (50th percentile), the required line indicates 90th  
 310 and 10th percentile, and the point indicates the 95th and 5th percentile.

311 During the study period, compared with that in other vegetation belts, the surface  
 312 isotopic value of the soil water in the mountain grasslands was relatively enriched  
 313 (-24.3‰,  $\delta^2\text{H}$ ; -0.8‰,  $\delta^{18}\text{O}$ ), the lc-excess was smaller and deeper into the middle  
 314 and lower soil layers (-25.8‰), and the gravimetric water content was relatively low  
 315 (8.4%). Due to the difference in vegetation types and the influence of reservoirs, this  
 316 change did not have an obvious elevation effect. Although the elevation was low, the  
 317 soil water of the deciduous forests had more depleted isotopic characteristics and  
 318 higher soil moisture than those of the mountain grasslands in most samples. Soil  
 319 profiles obtained from different vegetation zones can reflect the evaporation signals of  
 320 water. The low-temperature natural environment made alpine meadow soil less



321 affected by evaporation ( $lc\text{-excess} > -20\%$ ), and the gravimetric water content was  
 322 high (gravimetric water content  $> 20\%$ ) during the whole study period. The surface  
 323 soil water of the coniferous forests was easily affected by climate and had a higher  
 324 isotopic composition ( $-29.5\%$ ,  $\delta^2H$ ;  $-2.1\%$ ,  $\delta^{18}O$ ) and lower  $lc\text{-excess}$  ( $-26.3\%$ ).  
 325 Due to evaporation, soil water isotopes in the mountain grassland and deciduous  
 326 forest areas were enriched in the surface soil layer. In particular, in the mountain  
 327 grasslands, the average values of  $\delta^2H$  and  $\delta^{18}O$  in the 0-10 cm soil layer were as high  
 328 as  $-24.4\%$  and  $-1.2\%$ , respectively, and  $SWlc\text{-excess}$  was lower than  $-25\%$ , even  
 329 close to  $-40\%$  in some samples. In this case, the evaporation signals can easily  
 330 penetrate the deep soil, making the gravimetric water content values at all the  
 331 sampling sites lower than  $20\%$  (Fig. 4; Fig. 6).

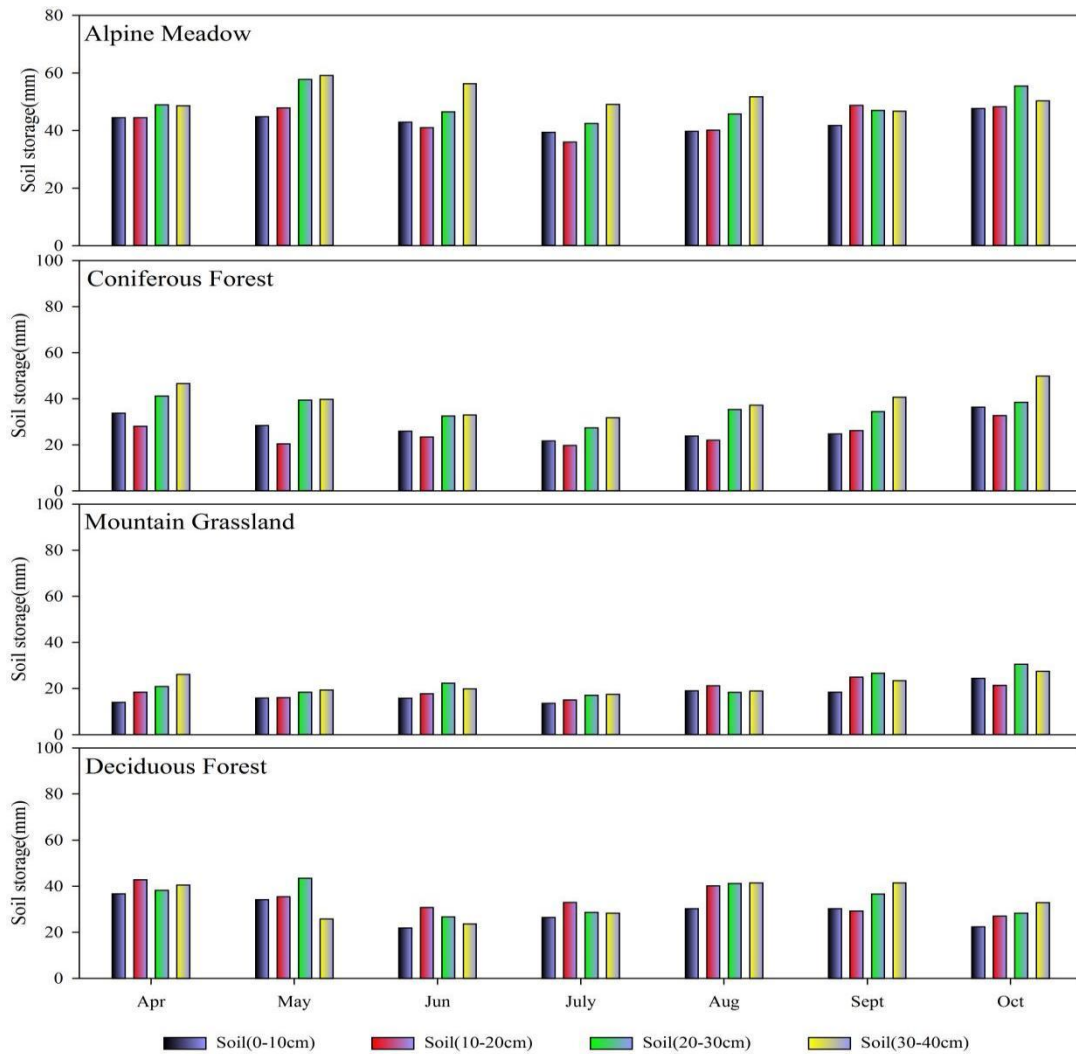


332  
 333 **Fig. 6** The variation of  $\delta^2H$ ,  $\delta^{18}O$ ,  $lc\text{-excess}$  and  $GWC$  in different vegetation zones  
 334 in each sampling

335 **4.4 Variations in the water storage capacity of the 0-40 cm soil layer in different**  
 336 **vegetation areas**

337 This study used soil water to calculate the water storage of the 0-40 cm soil layer

338 in the four vegetation zones during the observation period (Fig 7). The water storage  
339 capacity of the alpine meadow gradually decreased from April to July (209.7~167.2  
340 mm), and the water storage capacity increased after July (167.2~201.8 mm). The  
341 monthly average water storage capacity was the lowest at 0-10 cm (43.0 mm) and the  
342 highest at 30-40 cm (51.7 mm). The water storage capacity of the coniferous forest  
343 gradually decreased from April to July (150.1~101.2 mm), and the water storage  
344 capacity increased after July (101.2~160.0 mm). The monthly average water storage  
345 capacity was the lowest at 0-10 cm (28.0 mm) and the highest at 30-40 cm (40.0 mm).  
346 The water storage capacity of the mountain grassland gradually decreased from April  
347 to July (80.3~64.0 mm), and the water storage capacity increased after July  
348 (64.0~104.6 mm). The monthly average water storage capacity was the lowest at 0-10  
349 cm (17.5 mm) and the highest at 20-30 cm (22.0 mm). The water storage capacity of  
350 the deciduous forest gradually decreased from April to June (159.3~104.0 mm), the  
351 water storage capacity increased from June to August (104.0~154.0 mm), and there  
352 was a decrease from August to October (154.0~111.8 mm). The monthly average  
353 water storage capacity was the lowest at 0-10 cm (29.1 mm) and the highest at 20-30  
354 cm (35.0 mm). In general, the soil water storage capacity of the 0-10 cm soil layer  
355 was less than that of the other soil layers. The order of the water storage capacity of  
356 the 0-40 cm soil layer in the four vegetation zones is AM > DF > CF > MG.



357

358 **Fig. 7** Monthly variation of soil water storage in 0-40cm soil layer of different  
 359 vegetation zones

## 360 5. Discussion

### 361 5.1 Evaporation of soil moisture in different vegetation zones

362 In the arid river source area, the replenishment of soil moisture mainly comes  
 363 from precipitation. The slope of the regional atmospheric precipitation line can reflect  
 364 the strength of local evaporation. Due to a low atmospheric temperature, low cloud  
 365 base height, and low air-saturated water vapor loss, the alpine meadow zone was  
 366 weakly affected by secondary evaporation during precipitation. There, the slope of the  
 367 LMWL (8.4) was even higher than that of the GMWL (Zhang et al., 2012). As the  
 368 altitude decreased, the secondary evaporation under clouds strengthened, and the

369 slope of the LMWL of each vegetation zone decreased (Pang et al., 2011) (Fig 5). The  
370 dynamic changes in lc-excess of soil profiles in different vegetation areas reflect the  
371 process of soil water evaporation caused by drought during the study period. The  
372 monthly average value of SWlc-excess in the alpine meadow zone was less than 0,  
373 and the minimum value was -11.9‰ (July). Although the vegetation belt was subject  
374 to different degrees of evaporation each month, it was less affected by drought, and it  
375 was difficult for evaporation to penetrate into the middle and lower soil layers. The  
376 SWlc-excess of the coniferous forest belt was greater than that of the alpine meadow  
377 from April to June. The evaporation was the strongest in July (-11.2‰ lc-excess).  
378 Similar to in the alpine meadows, in the coniferous forest belt, evaporation mainly  
379 occurred in the topsoil. The vegetation coverage of the mountain grassland zone was  
380 low, and the arid environment made the isotopes of the surface soil produce strong  
381 evaporation signals (lc-excess was close to -40‰). In most samples, the SWlc-excess  
382 of the 60-80 cm soil layer was negative. The evaporation signal shifted to the lower  
383 layer of the soil (Zimmermann et al., 1966; Barnes and Allison, 1988). Similar  
384 evaporation signals have been found in the Mediterranean and arid climate regions  
385 (Sprenger et al., 2016b; McCutcheon et al., 2017). Evaporation signals exist in only  
386 the surface soil in humid areas, and there is no difference between lc-excess and 0 in  
387 the soil layer below 20 cm (Sprenger et al., 2017). The monthly surface soil  
388 evaporation of deciduous forests was less than that of mountain grasslands from April  
389 to June, and it was greater than that of mountain grasslands after July, mainly due to  
390 the influence of the vegetation and reservoirs. There were commonalities in the soil  
391 moisture changes in different vegetation zones characterized by more enriched  
392 isotopes, stronger evaporation signals, and lower moisture content in the shallow soil.  
393 With increasing soil depth, the isotope gradually became depleted, and the  
394 evaporation signal was gradually weakened until it disappeared. The evolution of the  
395 investigated isotopes, lc-excess, and gravimetric water content in the unsaturated soil  
396 showed differences among different vegetation zones. From a high altitude to a low  
397 altitude, the isotopic value of the surface gradually increased, and the evaporation  
398 signal increased (Fig 4; Fig 6).

## 399 **5.2 Memory effects of precipitation input, mixing and rewetting**

400 The changes in soil water isotopes and soil moisture can evaluate the input,  
401 mixing, and rewetting process of precipitation in different vegetation areas. The main  
402 methods of precipitation input are plug flow and preferential flow. Plug flow is the  
403 complete mixing of water through the soil matrix with shallow free water. Under the  
404 action of plug flow, precipitation infiltrates along the hydraulic gradient, pushing the  
405 original soil water downward. Preferential flow means that precipitation uses soil  
406 macropores to quickly penetrate shallow soil to form deep leakage (Tang and Feng,  
407 2001). After precipitation, the variability of isotope signals at a certain soil depth can  
408 identify the seepage method of water (Peralta-Tapia et al., 2015). During the study  
409 period, the soils of the alpine meadow and coniferous forest areas were seasonally  
410 frozen and thawed year-round, and the difference in the soil isotope profile was small.  
411 The soil moisture profile showed a trend of water increasing from top to bottom,  
412 indicating the influence of the previous precipitation. The soil was humid, so the  
413 replenishment of soil water by precipitation had the characteristics of top-down piston  
414 replenishment. Preferential infiltration showed high variability in isotopic signals  
415 (Brodersen et al., 2000), and the rainwater in mountain grasslands and deciduous  
416 forests flowed into the deep soil rapidly through the soil matrix via exposed soil  
417 fissures and roots. This resulted in the sudden depletion of soil isotopes at a depth of  
418 60-100 cm. This may be due to the more recent depleted precipitation that quickly  
419 reached this depth and the preferential infiltration into the soil. Water movement and  
420 mixing in the unsaturated zone can be observed in the spatiotemporal variation in  
421 isotopes within 1 m of the soil profile, and the alpine meadow and coniferous forest  
422 zones underwent considerable rainfall. After a short period of weak evaporation, the  
423 soil was rewetted by the next rainfall. In the alpine meadow, the soil moisture  
424 remained above 20% each month. The mountain grassland and deciduous forest zones  
425 had only sporadic precipitation from mid-May to late July, and the soil moisture  
426 evaporated rapidly. With the decrease in air temperature and the occurrence of  
427 continuous precipitation after July, the soil was rewetted after two months of drought,  
428 and both vegetation zones showed the replacement and mixing of soil water isotopes

429 and precipitation. The results showed that the soil water storage capacity of the alpine  
430 grassland was seriously insufficient, reflecting the incomplete rewetting of the soil by  
431 precipitation at the end of the study. In addition, low soil water storage capacity will  
432 enrich the remaining soil water isotopes (Zimmermann et al., 1966; Barnes and  
433 Allison, 1988). We observed the memory effect of soil rewetting caused by  
434 precipitation input and the mixing of different vegetation areas during the entire study  
435 period. The changes in soil moisture in each vegetation area reflect different climatic  
436 and hydrological characteristics (Fig. 4; Fig. 6).

### 437 **5.3 Influencing factors of soil water storage capacity in arid headwater areas**

438 As the temperature decreased rapidly with increasing height, precipitation and  
439 humidity increased to a certain extent, and the vegetation showed a strip-like  
440 alternation approximately parallel to the contour line, forming zonal vegetation with  
441 obvious differentiation (Yin et al., 2020). The dry-wet conditions of different  
442 vegetation zones restricted the soil water storage capacity in the basin. In the process  
443 of low-altitude vegetation zone replacement, the precipitation decreased, the  
444 temperature rose, the groundwater level dropped, and the soil water storage capacity  
445 was weak (Coussement et al., 2018; Kleine et al., 2020). The soil water storage  
446 capacity of the alpine meadow zone with low-temperature and rainy weather was  
447 higher than that of other vegetation zones (results of the 0-40 cm soil layers from  
448 April to October: AM: 187.8 mm; CF: 128.4 mm; MG: 81.2 mm; DF: 132.1 mm).  
449 During the study period, the soil water storage capacity (0-40 cm) exceeded 165 mm  
450 each month. With the decrease in altitude, the monthly difference in dry-wet  
451 conditions in each vegetation zone gradually became obvious. With the increase in  
452 temperature in summer, the environment became dry, and the soil water storage  
453 capacity weakened (Sprenger et al., 2017). The soil water storage capacity of the  
454 coniferous forest zone began to decrease in April, and the water storage capacity of  
455 the 0-40 cm layer reached the minimum value (101.2 mm) in July. The variation in  
456 temperature and precipitation was the main reason for the monthly difference  
457 (Dubber and Werner, 2019). Although there was a certain water storage capacity in  
458 the coniferous forests with some transpiration loss, the soil water storage capacity in

459 this vegetation zone was not strong. The water storage capacity of mountain grassland  
460 soil was lower than that of other vegetation zones. The continuous dry and warm  
461 weather in spring and summer led to the water storage capacity of 0-40 cm soil being  
462 lower than that of 100 mm every month. In particular, drought stress leads to  
463 insufficient soil moisture, making it difficult to maintain plant demand, resulting in  
464 sparse vegetation and large-scale exposed surface soil, which further accelerates  
465 surface water loss. The continuous precipitation from the end of July prevented  
466 further drought development, and the water input gradually restored the soil water  
467 storage capacity (Kleine et al., 2020). The deciduous forests had hydrothermal  
468 conditions similar to those of the mountain grasslands, but the soil porosity of the  
469 forest zone was obviously larger than that of the barren land, and its permeability was  
470 higher than that of the barren land. Precipitation infiltrated the ground through roots  
471 and turned into groundwater. The forest acted as a reservoir due to its strong water  
472 storage and soil conservation capacity (Sprenger et al., 2019). The water storage  
473 capacity of the 0-40 cm soil layer in the deciduous forest was higher than 100 mm at  
474 each sampling time. In addition, the water content of the 0-40 cm soil layer in each  
475 vegetation zone increased with the deepening of the soil layer, and the water storage  
476 capacity of the surface soil was weak. The difference in soil properties also led to  
477 more water storage in the middle and lower soil layers with higher clay contents  
478 (Heinrich et al., 2019) (Fig. 7). Climate warming and the spatiotemporal imbalance  
479 of water resources have disturbed the ecological-water balance of different vegetation  
480 zones in inland river source areas (Liu et al., 2015). Plant growth mainly depends on  
481 the water stored in shallow soil layers (Amin et al., 2020). Drought reduces soil water  
482 storage and inhibits plant growth (Li et al., 2020). To effectively improve and manage  
483 water resources in arid water source areas, exploring the heterogeneity among  
484 different vegetation zones is necessary. According to the basin's current climate,  
485 hydrology, and social economy, scientific and reasonable management policies should  
486 be formulated according to local conditions for different ecological-hydrological  
487 contradictions and extended to more areas.

## 488 **6. Conclusion**

489 This work provides further insights into the movement and mixing of soil water  
490 in different vegetation zones in arid source regions. During the study period, the  
491 dynamic changes in  $\delta^{13}C$ -excess in the soil profiles of different vegetation zones  
492 reflected the evaporation signals caused by drought. Soil water evaporation in spring  
493 and summer and insufficient precipitation during the drought period were the main  
494 driving forces of isotopic enrichment in the surface soil. The evaporation intensity  
495 results of the four vegetation zones followed the order of mountain grassland >  
496 deciduous forest > coniferous forest > alpine meadow. In the mountain grassland and  
497 deciduous forest zones, drought caused the evaporation signal to penetrate deep into  
498 the middle and lower soil layers. The  $\delta^{13}C$ -excess below 70 cm of the ground surface  
499 remained negative. Soil water isotopes and gravimetric water content record the  
500 process of soil rewetting caused by precipitation input and mixing. The alpine  
501 meadow and coniferous forest zones were enriched in precipitation. After a short  
502 period of weak evaporation, the soil was rewetted by the next precipitation event.  
503 There was only sporadic precipitation in the mountainous grassland and deciduous  
504 forest belt from mid-May to late July. After July, the temperature dropped, and  
505 continuous precipitation wet the soil again after two months of drought. The mountain  
506 grassland and deciduous forest zones had only sporadic precipitation from mid-May  
507 to late July. With the decrease in air temperature and continuous precipitation after  
508 July, the soil was rewetted after two months of drought. Moisture and temperature  
509 conditions were the key factors that restricted the soil water storage capacity in the  
510 different vegetation zones. The soil water storage capacity results followed the order  
511 of alpine meadow > deciduous forest > coniferous forest > mountainous grassland.  
512 The water storage capacity of the surface soil in each vegetation zone was weak, and  
513 more water was stored in the middle and lower soil layers with higher clay contents.  
514 This research is helpful to understand the hydrological cycle in different vegetation  
515 areas and can provide theoretical support for obtaining a regional ecological  
516 hydrological balance.



517 **Reference**

- 518 Allen, R. G., Pereira, L. S., Raes, D., & Smith, M. (1998). Crop evapotranspiration-Guidelines for  
519 computing crop water requirements-FAO Irrigation and drainage paper 56. Fao,  
520 Rome, 300(9), D05109.
- 521 Amin, A., Zuecco, G., Geris, J., Schwendenmann, L., McDonnell, J. J., Borga, M., & Penna, D.  
522 (2020). Depth distribution of soil water sourced by plants at the global scale: A new direct  
523 inference approach. *Ecohydrology*, 13(2), e2177.
- 524 Barnes, C. J., & Allison, G. B. (1988). Tracing of water movement in the unsaturated zone using  
525 stable isotopes of hydrogen and oxygen. *Journal of Hydrology*, 100(1-3), 143-176.
- 526 Brodersen, C., Pohl, S., Lindenlaub, M., Leibundgut, C., & Wilpert, K. V. (2000). Influence of  
527 vegetation structure on isotope content of throughfall and soil water. *Hydrological  
528 Processes*, 14(8), 1439-1448.
- 529 Brooks, J. R., Barnard, H. R., Coulombe, R., & McDonnell, J. J. (2010). Ecohydrologic separation  
530 of water between trees and streams in a Mediterranean climate. *Nature Geoscience*, 3(2),  
531 100-104.
- 532 Coussement, T., Maloteau, S., Pardon, P., Artru, S., Ridley, S., Javaux, M., & Garré, S. (2018). A  
533 tree-bordered field as a surrogate for agroforestry in temperate regions: Where does the water  
534 go?. *Agricultural Water Management*, 210, 198-207.
- 535 Dansgaard, W. (1964). Stable isotopes in precipitation. *tellus*, 16(4), 436-468.
- 536 Dubbert, M., & Werner, C. (2019). Water fluxes mediated by vegetation: emerging isotopic  
537 insights at the soil and atmosphere interfaces. *New Phytologist*, 221(4), 1754-1763.
- 538 Duvert, C., Stewart, M. K., Cendón, D. I., & Raiber, M. (2016). Time series of tritium, stable  
539 isotopes and chloride reveal short-term variations in groundwater contribution to a stream.  
540 *Hydrology and Earth System Sciences*, 20(1), 257-277.
- 541 Ferretti, D. F., Pendall, E., Morgan, J. A., Nelson, J. A., Lecain, D., & Mosier, A. R. (2003).  
542 Partitioning evapotranspiration fluxes from a Colorado grassland using stable isotopes:  
543 Seasonal variations and ecosystem implications of elevated atmospheric CO<sub>2</sub>. *Plant and  
544 Soil*, 254(2), 291-303.

545 Gibson, J. J., Holmes, T., Stadnyk, T. A., Birks, S. J., Eby, P., & Pietroniro, A. (2021). Isotopic  
546 constraints on water balance and evapotranspiration partitioning in gauged watersheds across  
547 Canada. *Journal of Hydrology: Regional Studies*, 37, 100878.

548 Grant, G. E., & Dietrich, W. E. (2017). The frontier beneath our feet. *Water Resources*  
549 *Research*, 53(4), 2605-2609.

550 Heinrich, I., Balanzategui, D., Bens, O., Blume, T., Brauer, A., Dietze, E., ... & Wille, C. (2019).  
551 Regionale Auswirkungen des Globalen Wandels: Der Extremsommer 2018 in  
552 Nordostdeutschland. *System Erde*, 9(1), 38-47.

553 Hsieh, J. C., Chadwick, O. A., Kelly, E. F., & Savin, S. M. (1998). Oxygen isotopic composition  
554 of soil water: quantifying evaporation and transpiration. *Geoderma*, 82(1-3), 269-293.

555 Kleine, L., Tetzlaff, D., Smith, A., Wang, H., & Soulsby, C. (2020). Using water stable isotopes to  
556 understand evaporation, moisture stress, and re-wetting in catchment forest and grassland  
557 soils of the summer drought of 2018. *Hydrology and Earth System Sciences*, 24(7),  
558 3737-3752.

559 Koeniger, P., Gaj, M., Beyer, M., & Himmelsbach, T. (2016). Review on soil water isotope-based  
560 groundwater recharge estimations. *Hydrological Processes*, 30(16), 2817-2834.

561 Landwehr, J. M., & Coplen, T. B. (2006). Line-conditioned excess: a new method for  
562 characterizing stable hydrogen and oxygen isotope ratios in hydrologic systems.  
563 In *International conference on isotopes in environmental studies* (pp. 132-135). Vienna:  
564 IAEA.

565 Landwehr, J. M., Coplen, T. B., & Stewart, D. W. (2014). Spatial, seasonal, and source variability  
566 in the stable oxygen and hydrogen isotopic composition of tap waters throughout the  
567 USA. *Hydrological Processes*, 28(21), 5382-5422.

568 Li, X., Piao, S., Wang, K., Wang, X., Wang, T., Ciais, P., ... & Peñuelas, J. (2020). Temporal  
569 trade-off between gymnosperm resistance and resilience increases forest sensitivity to  
570 extreme drought. *Nature Ecology & Evolution*, 4(8), 1075-1083.

571 Liu, Y., Liu, F., Xu, Z., Zhang, J., Wang, L., & An, S. (2015). Variations of soil water isotopes and  
572 effective contribution times of precipitation and throughfall to alpine soil water, in Wolong  
573 Nature Reserve, China. *Catena*, 126, 201-208.

574 Ma, X., Jia, W., Zhu, G., Ding, D., Pan, H., & Xu, X. (2018). Stable isotope composition of  
575 precipitation at different elevations in the monsoon marginal zone. *Quaternary International*,  
576 493(10), 86-95.

577 McCutcheon, R. J., McNamara, J. P., Kohn, M. J., & Evans, S. L. (2017). An evaluation of the  
578 ecohydrological separation hypothesis in a semiarid catchment. *Hydrological  
579 processes*, 31(4), 783-799.

580 Milly, P. C. D. (1994). Climate, soil water storage, and the average annual water balance. *Water  
581 Resources Research*, 30(7), 2143-2156.

582 Pang, Z., Kong, Y., Froehlich, K., Huang, T., Yuan, L., Li, Z., & Wang, F. (2011). Processes  
583 affecting isotopes in precipitation of an arid region. *Tellus B: Chemical and Physical  
584 Meteorology*, 63(3), 352-359.

585 Penna, D., Hopp, L., Scandellari, F., Allen, S. T., Benettin, P., Beyer, M., ... & Kirchner, J. W.  
586 (2018). Ideas and perspectives: Tracing terrestrial ecosystem water fluxes using hydrogen and  
587 oxygen stable isotopes—challenges and opportunities from an interdisciplinary  
588 perspective. *Biogeosciences*, 15(21), 6399-6415.

589 Penna, D., Stenni, B., Šanda, M., Wrede, S., Bogaard, T. A., Michelini, M., ... & Wassenaar, L. I.  
590 (2012). Evaluation of between-sample memory effects in the analysis of  $\delta^2\text{H}$  and  $\delta^{18}\text{O}$  of  
591 water samples measured by laser spectrometers. *Hydrology and Earth System Sciences*,  
592 16(10), 3925-3933.

593 Peralta-Tapia, A., Sponseller, R. A., Tetzlaff, D., Soulsby, C., & Laudon, H. (2015). Connecting  
594 precipitation inputs and soil flow pathways to stream water in contrasting boreal  
595 catchments. *Hydrological Processes*, 29(16), 3546-3555.

596 Qu, D., Tian, L., Zhao, H., Yao, P., Xu, B., & Cui, J. (2020). Demonstration of a memory  
597 calibration method in water isotope measurement by laser spectroscopy. *Rapid  
598 Communications in Mass Spectrometry*, 34(8), e8689.

599 Rothfuss, Y., & Javaux, M. (2017). Reviews and syntheses: Isotopic approaches to quantify root  
600 water uptake: a review and comparison of methods. *Biogeosciences*, 14(8), 2199-2224.

601 Sharma, H., Ehlers, T. A., Glotzbach, C., Schmid, M., & Tielbörger, K. (2021). Effect of rock  
602 uplift and Milankovitch timescale variations in precipitation and vegetation cover on  
603 catchment erosion rates. *Earth Surface Dynamics*, 9(4), 1045-1072.

604 Snelgrove, J. R., Buttle, J. M., Kohn, M. J., & Tetzlaff, D. (2021). Co-evolution of xylem water  
605 and soil water stable isotopic composition in a northern mixed forest biome. *Hydrology and*  
606 *Earth System Sciences*, 25(4), 2169-2186.

607 Sprenger, M., Erhardt, M., Riedel, M., & Weiler, M. (2016a). Historical tracking of nitrate in  
608 contrasting vineyards using water isotopes and nitrate depth profiles. *Agriculture,*  
609 *Ecosystems & Environment*, 222, 185-192.

610 Sprenger, M., Leistert, H., Gimbel, K., & Weiler, M. (2016b). Illuminating hydrological processes  
611 at the soil-vegetation-atmosphere interface with water stable isotopes. *Reviews of*  
612 *Geophysics*, 54(3), 674-704.

613 Sprenger, M., Tetzlaff, D., & Soulsby, C. (2017). Soil water stable isotopes reveal evaporation  
614 dynamics at the soil–plant–atmosphere interface of the critical zone. *Hydrology and Earth*  
615 *System Sciences*, 21(7), 3839-3858.

616 Sprenger, M., Llorens, P., Cayuela, C., Gallart, F., & Latron, J. (2019). Mechanisms of  
617 consistently disjunct soil water pools over (pore) space and time. *Hydrology and Earth*  
618 *System Sciences*, 23(6), 2751-2762.

619 Stumpp, C., Stichler, W., Kandolf, M., & Šimůnek, J. (2012). Effects of land cover and  
620 fertilization method on water flow and solute transport in five lysimeters: A long-term study  
621 using stable water isotopes. *Vadose Zone Journal*, 11(1).

622 Tang, K., & Feng, X. (2001). The effect of soil hydrology on the oxygen and hydrogen isotopic  
623 compositions of plants' source water. *Earth and Planetary Science Letters*, 185(3-4), 355-367.

624 Tetzlaff, D., Soulsby, C., Buttle, J., Capell, R., Carey, S. K., Laudon, H., ... & Shanley, J. (2013).  
625 Catchments on the cusp? Structural and functional change in northern  
626 ecohydrology. *Hydrological Processes*, 27(5), 766-774.

627 Xiao, W., Wei, Z., & Wen, X. (2018). Evapotranspiration partitioning at the ecosystem scale using  
628 the stable isotope method—A review. *Agricultural and Forest Meteorology*, 263, 346-361.

629 Yin, L. , Dai, E. , Zheng, D. , Wang, Y. , & Tong, M. . (2020). What drives the vegetation  
630 dynamics in the hengduan mountain region, southwest china: climate change or human  
631 activity?. *Ecological Indicators*, 112, 106013.

632 Zhang, X. P., Guan, H. D., Sun, Z. A., Sun, G. L., Zhang, X. Z., & Wu, H. W. (2012). Simulations  
633 of stable isotopic variations in precipitation and comparison with measured values in Yunnan  
634 Province, China. *Scientia Geographica Sinica*, 32(1), 121-128.

635 Zhu, G., Yong, L., Zhang, Z., Sun, Z., Sang, L., Liu, Y., ... & Guo, H. (2021a). Infiltration process  
636 of irrigation water in oasis farmland and its enlightenment to optimization of irrigation mode:  
637 Based on stable isotope data. *Agricultural Water Management* , 258 , 107173.

638 Zhu, G., Yong, L., Zhang, Z., Sun, Z., Wan, Q., Xu, Y., ... & Guo, H. (2021b). Effects of plastic  
639 mulch on soil water migration in arid oasis farmland: Evidence of stable isotopes. *CATENA* ,  
640 207 , 105580.

641 Zimmermann, U., Münnich, K. O., Roether, W., Kreutz, W., Schubach, K., & Siegel, O. (1966).  
642 Tracers determine movement of soil moisture and evapotranspiration. *Science*, 152(3720),  
643 346-347.

#### 644 **Acknowledgments**

645 This research was financially supported by the National Natural Science  
646 Foundation of China (41661005, 41867030, 41971036). The authors much thank the  
647 colleagues in the Northwest Normal University for their help in fieldwork, laboratory  
648 analysis, data processing.

#### 649 **Author Contribution statement**

650 Guofeng Zhu and Leilei Yong conceived the idea of the study; Yuanxiao Xu and  
651 Qiaozhuo Wan analyzed the data; Zhigang Sun and Leilei Yong were responsible for  
652 field sampling; Zhuanxia Zhang participated in the experiment; Lei Wang participated  
653 in the drawing; Leilei Yong wrote the paper; Liyuan Sang and Yuwei Liu checked and  
654 edited language. All authors discussed the results and revised the manuscript.

#### 655 **Additional Information**

656 Competing Interests: The authors declare no competing interests.